

From Poses to Identity: Training-Free Person Re-Identification via Feature Centralization

Chao Yuan^{1,*}, Guiwei Zhang^{1,*}, Changxiao Ma¹, Tianyi Zhang², Guanglin Niu^{2,†}

¹ School of Computer Science and Engineering, Beihang University

² School of Artificial Intelligence, Beihang University

yuanc3666@gmail.com, {zhangguiwei, cxma124, zy2442222, beihangnlg1}@buaa.edu.cn

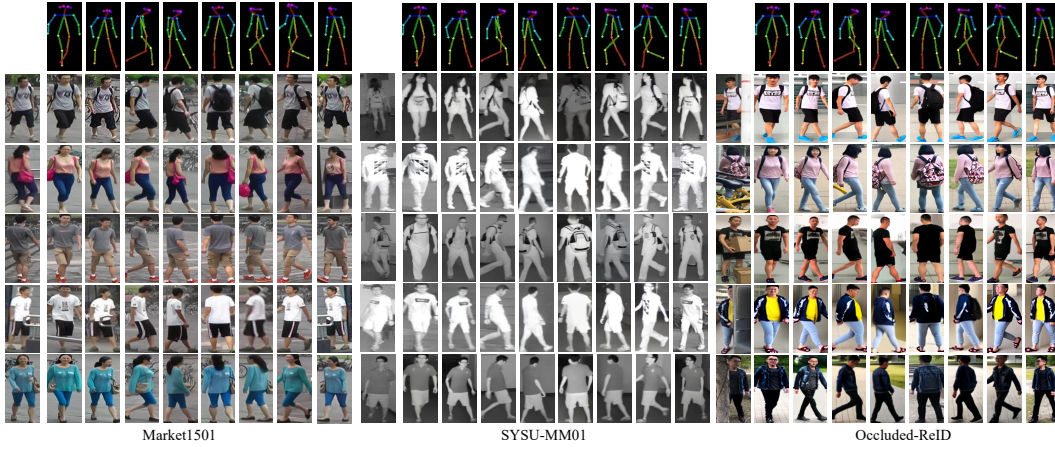


Figure 1. Visualization of our Identity-Guided Pedestrian Generation model with 8 representative poses on three datasets.

Abstract

Person re-identification (ReID) aims to extract accurate identity representation features. However, during feature extraction, individual samples are inevitably affected by noise (background, occlusions, and model limitations). Considering that features from the same identity follow a normal distribution around identity centers after training, we propose a **Training-Free Feature Centralization ReID** framework (**Pose2ID**) by aggregating the same identity features to reduce individual noise and enhance the stability of identity representation, which preserves the feature’s original distribution for following strategies such as re-ranking. Specifically, to obtain samples of the same identity, we introduce two components: ① **Identity-Guided Pedestrian Generation**: by leveraging identity features to guide the generation process, we obtain high-quality images with diverse poses, ensuring identity consistency even in complex scenarios such as infrared, and occlusion. ② **Neighbor Feature Centralization**: it explores each sample’s potential posi-

tive samples from its neighborhood. Experiments demonstrate that our generative model exhibits strong generalization capabilities and maintains high identity consistency. With the Feature Centralization framework, we achieve impressive performance even with an ImageNet pre-trained model without ReID training, reaching mAP/Rank-1 of 52.81/78.92 on Market1501. Moreover, our method sets new state-of-the-art results across standard, cross-modality, and occluded ReID tasks, showcasing strong adaptability.

1. Introduction

Person re-identification (ReID) is a critical task in video surveillance and security, aiming to match pedestrian images captured from different cameras. Despite significant progress made in recent years through designing more complex models with increased parameters and feature dimensions, inevitable noise arises due to poor image quality or inherent limitations of the models, reducing the accuracy of identity recognition and affecting retrieval performance.

To address this challenge, we propose a training-free

† Corresponding author. * Equal contribution.

Codes: <https://github.com/yuanc3/Pose2ID>

ReID framework that fully leverages capabilities of existing models by mitigating feature noise to enhance identity representation. During training, features of the same identity are constrained by the loss function and naturally aggregate around an "identity center" in the feature space. Particularly, according to the central limit theorem, when the number of samples is sufficiently large, these features would follow a normal distribution with identity center as the mean. As shown in Fig. 2, we visualize the feature distribution of an identity, and rank samples of the same identity with distance to their identity center. Therefore, we introduce the concept of feature centralization. To make each sample's feature more representative of its identity, by aggregating features of the same identity, we can reduce the noise in individual samples, strengthen identity characteristics, and bring each feature dimension closer to its central value.

However, obtaining diverse samples of the same identity is hard without identity labels. With the development of generative models, generating images of the same identity in different poses has become feasible. Previous GAN-based studies [13, 43, 72, 73] struggle with limited effectiveness, and mainly serve to augment training data. With breakthroughs in diffusion models for image generation [2, 19, 66], it is now possible to generate high-quality, multi-pose images of the same person. However, these methods lack effective control over identity features and generated pedestrian images are susceptible to interference from background or occlusions, making it difficult to ensure identity consistency across poses. Therefore, we utilize identity features of ReID, proposing an Identity-Guided Pedestrian Generation paradigm. Guided by identity features, we generate high-quality images of the same person with a high degree of identity consistency across diverse scenarios (visible, infrared, and occluded).

Furthermore, inspired by re-ranking mechanisms[74], we explore potential positive samples through feature distance matrices to further achieve feature centralization. Unlike traditional re-ranking methods that modify features or distances in a one-off manner, our approach performs L2 normalization after enhancement. This preserves the original feature distribution while improving representation quality and can be combined with re-ranking methods.

Thus, the main contributions of this paper include:

- **Training-Free Feature Centralization** framework that can be directly applied to different ReID tasks/models, even an ImageNet pretrained ViT without ReID training;
- **Identity-Guided Pedestrian Generation (IPG)** paradigm, leveraging identity features to generate high-quality images of the same identity in different poses to achieve feature centralization;
- **Neighbor Feature Centralization (NFC)** based on sample's neighborhood, discovering hidden positive samples from gallery/query set to achieve feature centralization.

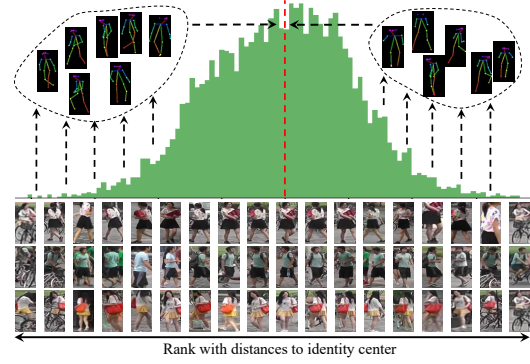


Figure 2. The real feature distribution of images from the same ID extracted by TransReID, and the main idea of our work is to make features closer/centralized to the ID center.

2. Related works

Person Re-Identification Person re-identification (ReID) is a critical task in computer vision that focuses on identifying individuals across different camera views. It plays a significant role in surveillance and security applications. Recent advancements in ReID have leveraged deep learning techniques to enhance performance, particularly using convolutional neural networks (CNNs[29]) and vision transformers (ViTs [2]). The deep learning based methods[3, 11, 17, 30, 35, 48, 64, 65] that focus on feature extraction and metric learning[18, 28, 34, 62] have improved feature extraction by learning robust and discriminative embeddings that capture identity-specific information.

Standard datasets like Market-1501 [70] have been widely used to benchmark ReID algorithms under normal conditions. Moreover, there are some challenging scenarios such as occlusions and cross-modality matching. Occluded-REID [78] addresses the difficulties of identifying partially obscured individuals, while SYSU-MM01 [55] focuses on matching identities between visible and infrared images, crucial for nighttime surveillance.

Feature Enhancement in Re-Identification Extracting robust feature representations is one of the key challenges in re-identification. Feature enhancement could help the ReID model easily differentiate between two people. Data augmentation techniques[40, 41, 76] were enhanced for feature enhancement. By increasing the diversity of training data, ReID model could extract robust and discriminative features.

Apart from improving the quality of the generated images, some Gan-based methods couple feature extraction and data generation end-to-end to distill identity related feature. FD-GAN[13] separates identity from the pose by generating images across multiple poses, enhancing the ReID

system’s robustness to pose changes. Zheng et al.[73] separately encodes each person into an appearance code and a structure code. Eom et al.[8] propose to disentangle identity-related and identity-unrelated features from person images. However, GAN-based methods face challenges such as training instability and mode collapse, which may not keep identity consistency.

In addition, the re-ranking technique refines feature-based distances to improve ReID accuracy. Such as k-Reciprocal Encoding Re-ranking[74], which improves retrieval accuracy by leveraging the mutual neighbors between images to refine the distance metric.

Person Generation Models Recent approaches have incorporated generative models, particularly generative adversarial networks (GANs) [14], to augment ReID data or enhance feature quality. Style transfer GAN-based methods[7, 21, 42, 75] transfer labeled training images to artificially generated images in different camera domains, background domains or RGB-infrared domains. Pose-transfer GAN-based methods[5, 36, 43, 45, 63] enable the synthesis of person images with variations in pose and appearance, enriching the dataset and making feature representations more robust to changes in poses. Random generation GAN-based methods [1, 23, 72] generate random images of persons and use Label Smooth Regularization (LSR [50]) or other methods to automatically label them. However, these methods often struggle to maintain identity consistency in pose variation, as generated images are susceptible to identity drift. The emergence of diffusion models has advanced the field of generative modeling, showing remarkable results in image generation tasks [19]. Leveraging the capabilities of pre-trained models like Stable Diffusion [44], researchers have developed techniques[4, 66] to generate high-quality human images conditioned on 2D human poses. Such as ControlNet[66], which integrates conditional control into diffusion models, allowing precise manipulation of generated images based on pose inputs.

3. Methods

The main purpose of this paper is to **centralize features to their identity center** to enhance the identity representation of feature vectors extracted by ReID model, that is, reducing noise within the features while increasing the identity attributes to make them more representative of their identities. Therefore, to effectively and reasonably enhance the features, we need to understand the characteristics of the feature vectors obtained by ReID model.

3.1. Feature Distribution Analysis

Currently, ReID models commonly use cross-entropy loss to impose ID-level constraints, and contrastive losses (such

as triplet loss) to bring features of the same ID closer while pushing apart features of different IDs. Some models also utilize center loss to construct identity centers for dynamically constraining the IDs. These methods lead to one common result: feature aggregation. One can say that the current ReID task is essentially a feature aggregation task. The degree of feature density (e.g. t-SNE visualization) is also widely used to measure model performance. It is easy to deduce that the features of the same ID are centered around a "mean," approximately forming a normal distribution, as the distribution shown in Fig.2 which is visualized with one single feature dimension of the same ID.

It is evident that ReID features are normally distributed around the ‘identity center’. To theoretically prove that the feature vectors of each ID in current ReID tasks aggregation around a center or mean, we analyze several commonly used loss functions and their impact on the feature distribution in **Supplementary**.

For the same identity $y_i = j$, we have a large number of samples $\{\mathbf{x}_i\}_{i=1}^{N_j}$, where N_j is the number of samples for ID j . These samples are passed through a ReID model $f(\cdot)$, resulting in the corresponding feature vectors $\{\mathbf{f}_i\}_{i=1}^{N_j}$:

$$\mathbf{f}_i = f(\mathbf{x}_i) \quad (1)$$

where $\mathbf{f}_i \in \mathbb{R}^d$ is the feature vector of sample \mathbf{x}_i , and d is the dimensionality of the feature space.

For each feature dimension k of the feature vector \mathbf{f}_i , the values $\{\mathbf{f}_{i,k}\}_{i=1}^{N_j}$ obtained from different samples of the same ID j is independent and identically distributed random variables. Here, $\mathbf{f}_{i,k}$ represents the k -th dimension of the feature vector for the i -th sample.

Since the input samples $\{\mathbf{x}_i\}_{i=1}^{N_j}$ are independent, the values of $\mathbf{f}_{i,k}$ are independent factors. According to the Central Limit Theorem (CLT), when the number of independent factors is large, the distribution of the values $\{\mathbf{f}_{i,k}\}_{i=1}^{N_j}$ for any dimension k of the feature vector will approximate a normal distribution. Thus, for each feature dimension k , we have:

$$\mathbf{f}_{i,k} \sim \mathcal{N}(\mu_k, \sigma_k^2) \quad (2)$$

where μ_k is the mean of the k -th feature dimension for ID j , and σ_k^2 is the variance of feature values in this dimension.

Since each dimension $\mathbf{f}_{i,k}$ of the feature vector approximately follows a normal distribution across samples, the entire feature vector \mathbf{f}_i for ID j can be approximated by a multivariate normal distribution. This gives:

$$\mathbf{f}_i \sim \mathcal{N}(\boldsymbol{\mu}, \boldsymbol{\Sigma}) \quad (3)$$

where $\boldsymbol{\mu} = (\mu_1, \mu_2, \dots, \mu_d)^\top$ is the mean vector of the feature dimensions, and $\boldsymbol{\Sigma}$ is the covariance matrix.

The theoretical analysis above suggests that under the optimization of the loss functions, the ReID model’s feature vectors \mathbf{x}_i aggregated around their identity centers \mathbf{c}_{y_i}

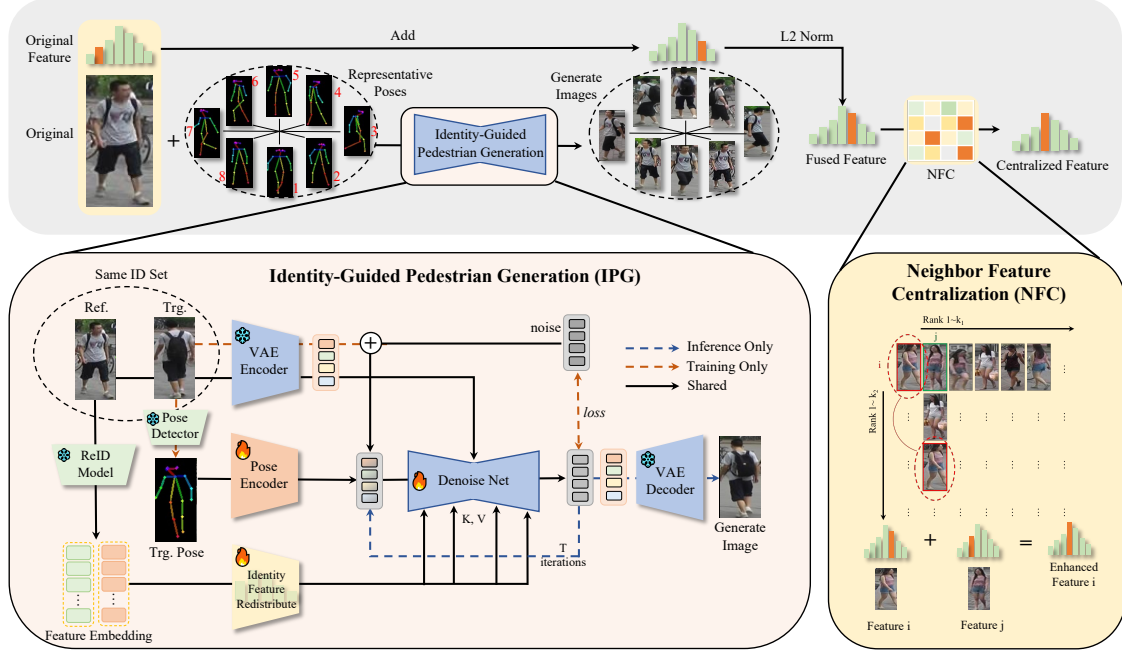


Figure 3. Overview of the proposed Feature Centralization framework for the ReID task.

following a normal distribution. This is consistent with the feature aggregation observed in t-SNE visualizations.

Identity Density (ID^2) Metric Identity density is one aspect of measuring ReID effectiveness. However, there is currently no quantitative metric for this, and researchers commonly rely on visualization tools like t-SNE to demonstrate model performance. By using the concept above, we propose an Identity Density (ID^2) Metric which is detailed in **Supplementary**.

3.2. Feature Centralization via Identity-Guided Pedestrian Generation

3.2.1. Feature Centralization

Since features of the same identity follow a multivariate normal distribution, we can simply **aggregate features of the same identity to approximate the identity center**, as the visualization in Fig.2. Thus, our main purpose becomes how to get more samples of the same identity to help centralize features.

A straightforward approach is to perform horizontal flipping on the original images, and add features together. It is worth noting for reviewers that this is a very simple but effective trick. Therefore, it is necessary to check whether performance improvements are due to such tricks. In our experiments, to demonstrate the advancement of our approach, we did not use this trick. If used, it may be better.

3.2.2. Identity-Guided Diffusion Process

To get more samples from the same identity, we propose a novel Identity-Guided Pedestrian Generation (IPG) paradigm, generating images of the same identity with different poses using a Stable Diffusion model guided by identity feature to centralize each sample’s features.

Followed by Stable Diffusion [44], which is developed from latent diffusion model (LDM). We use the reference UNet to inject the reference image features into the diffusion process with a constant timestep $t = 0$, and the denoising UNet ϵ_θ to generate the target image latent \mathbf{z}_0 by denoising the noisy latent $\mathbf{z}_T = \epsilon$:

$$\mathbf{z}_{t-1} = \epsilon_\theta(\mathbf{z}_t, t, \mathbf{E}_{\text{pose}}, \mathbf{H}), t \in [0, T] \quad (4)$$

where \mathbf{H} is the identity feature information to guide model keep person identity. \mathbf{E}_{pose} is the pose features.

At each timestep t , the pose feature \mathbf{E}_{pose} and conditioning embedding \mathbf{H} guide the denoising process.

Identity Feature Redistribute (IFR) The Identity Feature Redistribute (IFR) module aims to utilize identity features from input images, removing noise to better guide the generative model. It converts high-dimensional identity features into meaningful low-dimensional feature blocks, enhancing the model’s feature utilization efficiency.

Given the input sample $\mathbf{x} \in \mathbb{R}^C$ by a ReID model $f(\cdot)$, with IFR, we can obtain a re-distributed robust feature $\mathbf{H} \in \mathbb{R}^{N \times D}$:

$$\mathbf{H} = \text{IFR}(f(\mathbf{x})) = \text{LN}(\text{Linear}(f)) \quad (5)$$

For this more robust feature identity feature, it is used as the K, V of the model’s attention module to guide the model’s attention to the identity feature.

Pose Encoder The Pose Encoder is to extract high-dimensional pose embeddings \mathbf{E}_{pose} from input poses. It has 4 blocks with 16,32,64,128 channels. Each block applies a normal 3×3 Conv, a 3×3 Conv with stride 2 to reduce spatial dimensions, and followed by a SiLU activate function. Subsequently, the pose features are added to the noise latent before into the denoising UNet, follows [20].

Training Strategy For each identity i , we randomly select one image from S_i^{ref} as the reference image and one image from S_i^{trg} as the target image for training.

Let $\mathbf{x}_{i,j}^{\text{ref}} \in S_i^{\text{ref}}$ denote the reference image (i.e. j_{th} image of the i_{th} ID) and $\mathbf{x}_{i,j}^{\text{trg}} \in S_i^{\text{trg}}$ denote the target image. Model is trained using the mean squared error (MSE) loss between the predicted noise and the true noise.

$$\mathcal{L} = \mathbb{E}_{\mathbf{z}, t, \epsilon} \left[\|\epsilon - \epsilon\theta(\mathbf{z}_t, t, \mathbf{E}_{\text{pose}}, \mathbf{H})\|^2 \right] \quad (6)$$

where $\mathbf{z} = \text{VAE}(\mathbf{x}_{i,j}^{\text{trg}}) + \epsilon$ is a latent obtained by a pre-trained VAE encoder[26], \mathbf{E}_{pose} is the pose feature of $\mathbf{x}_{i,j}^{\text{trg}}$, \mathbf{H} is the re-distributed identity feature of $(\mathbf{x}_{i,j}^{\text{ref}})$.

The model is trained to learn the mapping from the reference image \mathbf{x}_{ref} to the target image \mathbf{x}_{trg} , with the goal of generating realistic variations in pose while preserving identity feature. This random selection ensures diversity during training, as different combinations of reference and target images are used in each training iteration, enhancing the model’s ability to generalize across various poses and viewpoints.

3.2.3. Selection of Representative Pose

In ReID tasks, features extracted from different poses of the same identity can vary significantly. Some specific poses tend to be more representative of that identity. As the conclusion of feature distribution in section 3.1, we calculate the identity center for IDs with all of its samples in datasets, and select the image whose feature is the closest to the center. The pose of this image is regarded as the representative pose. By randomly selecting 8 representative poses with different directions, we generate images that are more representative of the person’s identity.

That is, given a set of feature vectors $\mathbf{F}_{\text{all}} = \{\mathbf{f}_1, \mathbf{f}_2, \dots, \mathbf{f}_N\}$ for a particular identity:

$$\mathbf{f}_{\text{mean}} = \frac{1}{N} \sum_{i=1}^N \mathbf{f}_i \quad (7)$$

$$\text{pose} = \arg \min_i d(\mathbf{f}_{\text{mean}}, \mathbf{f}_i) \quad (8)$$

3.2.4. Feature Centralization Enhancement

Once we got generated images with different poses, we generate new images $\hat{\mathbf{x}}$ for each of these poses. The features

extracted from these generated images are then aggregated with the original reference feature to enhance the overall representation. The centralized feature $\tilde{\mathbf{f}}$ is computed as:

$$\tilde{\mathbf{f}} = \|\mathbf{f} + \frac{\eta}{M} \sum_{i=1}^M \mathbf{f}_i\|_2 \quad (9)$$

where \mathbf{f} is the feature of the original reference image, and \mathbf{f}_i are the features extracted from the M generated images. The coefficient η is introduced to adjust based on the quality of generated images. According to the theory of Section 3.1, low-quality generated images, as long as they contain corresponding identity information, can also be applied with feature enhancement, and use η to regulate the enhancement effect of generated information. As discussed in [72], even if quality is poor, it still contains ID information.

3.3. Neighbor Feature Centralization (NFC)

Moreover, we proposed a **Neighbor Feature Centralization (NFC)** algorithm to reduce noise in individual features and improve their identity discriminability in unlabeled scenarios. The core idea of the algorithm is to utilize mutual nearest-neighbor features for aggregation.

Algorithm 1 Neighbor Feature Centralization (NFC)

Require: Feature vectors $\{\mathbf{z}_i\}_{i=1}^N$, parameters k_1, k_2

Ensure: Centralized feature vectors $\{\mathbf{z}_i^{\text{centralized}}\}_{i=1}^N$

```

1: Compute pairwise distance matrix  $\mathbf{D} = [d_{ij}]$ 
2: for  $i = 1$  to  $N$  do
3:   Set  $d_{ii} = C$  ▷ Avoid self-matching
4: end for
5: for  $i = 1$  to  $N$  do
6:    $\mathcal{N}_i \leftarrow$  indices of top  $k_1$  neighbors of  $\mathbf{z}_i$ 
7: end for
8: for  $i = 1$  to  $N$  do
9:    $\mathcal{M}_i \leftarrow \emptyset$ 
10:  for each  $j \in \mathcal{N}_i$  do
11:     $\mathcal{N}_j^{k_2} \leftarrow$  indices of top  $k_2$  neighbors of  $\mathbf{z}_j$ 
12:    if  $i \in \mathcal{N}_j^{k_2}$  then
13:       $\mathcal{M}_i \leftarrow \mathcal{M}_i \cup \{j\}$ 
14:    end if
15:  end for
16: end for
17: for  $i = 1$  to  $N$  do
18:    $\mathbf{z}_i^{\text{centralized}} \leftarrow \mathbf{z}_i + \sum_{j \in \mathcal{M}_i} \mathbf{z}_j$ 
19: end for
```

By enhancing each feature with its potential neighbors, it could effectively approximate features of the same identity without explicit labels, and ensure that only features have high similarity relationships contribute to the enhancement.

Dataset		Model	Venue	Base	Method	mAP \uparrow	Rank-1 \uparrow	ID $^2\downarrow$	
Market1501		TransReID[16](w/o camid)	ICCV21	ViT	official	79.88	91.48	0.2193	
					+ours	90.39(+10.51)	94.74(+3.26)	0.1357	
		TransReID[16](w/ camid)			official	89	95.1	0.2759	
					+ours	93.01(+4.01)	95.52(+0.42)	0.1967	
		CLIP-ReID[31]	AAAI23	ViT	official	89.7	95.4	0.0993	
						+ours	94(+4.3)	96.4(+1.0)	0.0624
				CNN	official	89.8	95.7	0.0877	
						+ours	94.9(+5.1)	97.3(+1.6)	0.053
Occluded-ReID		KPR[47]	ECCV24	ViT	official	79.05	85.4	0.3124	
				+ours	89.34(+10.29)	91(+5.6)	0.1434		
		BPBREID[46]	WACV23	ViT	official	70.41	77.2	0.377	
						+ours	86.05(+15.64)	89.1(+11.9)	0.1504
SYSU-MM01	All	SAAI[9]	ICCV23	CNN	official	71.81	75.29	0.4817	
						+ours	76.44(+4.63)	79.33(+4.04)	0.4072
	Indoor					official	84.6	81.59	0.4424
						+ours	86.83(+2.23)	84.2(+2.61)	0.3694
	All	PMT[38]	AAAI23	ViT	official	66.13	67.7	0.4308	
						+ours	75.43(+9.3)	74.81(+7.11)	0.3133
	Indoor					official	77.81	72.95	0.4046
						+ours	84.29(+6.48)	80.29(+7.34)	0.2995

Table 1. Improvements with our method on different SOTA models with both ViT and CNN backbone on Market1501, SYSU-MM01, and Occluded-ReID datasets. The data under grey is the new SOTA with our methods of that dataset.

Methods	mAP \uparrow	Rank-1 \uparrow	ID $^2\downarrow$	Gallery ^{NFC}	Query ^{NFC}	mAP \uparrow	Rank-1 \uparrow	Gallery ^{IPG}	Query ^{IPG}	mAP \uparrow	Rank-1 \uparrow
Base	79.88	91.48	0.2193	\times	\times	79.88	91.48	\times	\times	79.88	91.48
+NFC	83.92	91.83	0.1824	\checkmark	\times	81.70	92.04	\checkmark	\times	84.65	92.07
+IPG	88.02	94.77	0.1553	\times	\checkmark	82.76	91.69	\times	\checkmark	82.18	92.40
+NFC+IPG	90.39	94.74	0.1357	\checkmark	\checkmark	83.92	91.83	\checkmark	\checkmark	88.02	94.77

Table 2. Ablation study on effects of feature centralization through Identity-Guided Pedestrian Generation (IPG) and Neighbor Feature Centralization (NFC).

Table 3. Ablation study of Neighbor Feature Centralization (NFC) Algorithm on Market1501 dataset. We test on the gallery and query set respectively.

Table 4. Ablation study of Feature ID-Centralizing with Pedestrian Generation (IPG) on Market1501. We test on gallery and query set respectively.

Method	mAP \uparrow	R1 \uparrow	R5 \uparrow	R10 \uparrow	ID $^2\downarrow$
w/o training	3.34	11.4	21.88	28	0.5135
+IPG	52.81	78.92	91.21	94.27	0.2158
+IPG+NFC	57.27	82.39	90.17	92.81	0.1890

Table 5. ReID performance on Market1501 with only ImageNet pre-trained weights without ReID training. The distribution visualized in Fig.4.

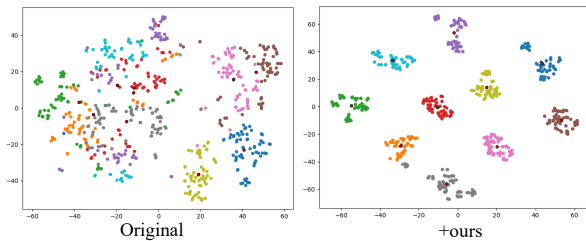


Figure 4. t-SNE visualization of 10 IDs feature distribution with and without our method on ImageNet pre-trained weights.

4. Experiments

4.1. Implementation Details

Data Cleaning. Training an effective generative model requires high-quality data support. In current ReID (Person Re-Identification) datasets, there are many low-quality images, and removing them can help reduce interference to the model. In our experiments, we found two main issues that need to be addressed: **Extremely Low-quality Images:** The dataset contains images with such low resolution that even the human eye cannot recognize them as a "person". **Pose Estimation Failures:** The pose estimation model inevitably fails to detect pedestrian poses in some images.

Utilizing the feature distribution mentioned in Section 3.1, we can solve the issues and get the reference image set S_i^{ref} and target image set S_i^{tgt} of identity i . The cleansing process is detailed in **Supplementary**.

Identity-guided Pedestrian Generation model details For the reference UNet and denoising UNet, we use the pre-trained weights of Stable Diffusion v1.5[44]. The VAE

encoder and decoder initialized with official weights[26] and froze. For the ReID model, we use pre-trained TransReID[16] without cameras on Market1501 and freeze.

The training data collected from training set of Market1501[70], Mars[71], MSMT17[54] and SYSU-MM01[55], with a total of 1946 different IDs. The model was trained for 80,000 iterations on one L20(48G) GPU with batch size of 4, which costs about 20 hours, and optimized by Adam[27] with a learning rate of $1e-5$ and weight decay of 0.01. All images are resized to 512×256 . We applied random flip and random erasing[76] data augmentation only on reference images.

According to Section 3.2.3, we selected 8 poses on the market1501 dataset as the representative poses. Each image in test set generates 8 images with these representative poses. The generation uses DDIM with 20 steps, classifier-free guidance with a scale of 3.5, and generator seed of 42.

ReID test settings Test models are loaded with official open-source pre-trained models for testing. In addition, considering the generated images do not have camera IDs, so for feature consistency, we test without camera IDs (e.g. TransReID). To validate the effectiveness of our proposed method, image flip (Section 3.2.1) trick is **NOT** applied in our experiments. On Market1501, set $\eta = 2$, and $k_1 = k_2 = 2$. On Occluded REID, set $\eta = 1$, and $k_1 = k_2 = 1$. On SYSU-MM01, set $\eta = 1/4$, and $k_1 = k_2 = 2$. The parameters analysis detailed in **Supplementary**.

4.2. Improvements on State-of-the-art Methods

To verify the exceptional feature enhancement performance of our framework, we selected state-of-the-art models of three ReID tasks, divided into CNN and ViT-based models, to demonstrate that our theory can apply to any model and various ReID tasks. As shown in Table.1, we achieved excellent enhancements on different models.

It is worth mentioning that we help models achieve new **SOTAs** without re-rank on 3 benchmarks:

- **CNN-base CLIP-ReID on market1501:**
mAP 94.9%, Rank-1 97.3%.
- **KPR on Occluded-ReID:**
mAP 89.34%, Rank-1 91%
- **SAAI on SYSU-MM01:**
All-search mode: mAP 76.44%, Rank-1 79.33%
Indoor-search mode: mAP 86.83%, Rank-1 84.2%

4.3. ReID without Training

TransReID loads a ViT pre-trained model on ImageNet for training on the ReID task. The pre-training method is based on contrastive learning strategies. According to the description in Section 3.1, training with contrastive loss helps to cluster features of same label samples. Images generated by our Pedestrian Generation model exhibit identity consistency, meaning they possess the attributes of the same label.

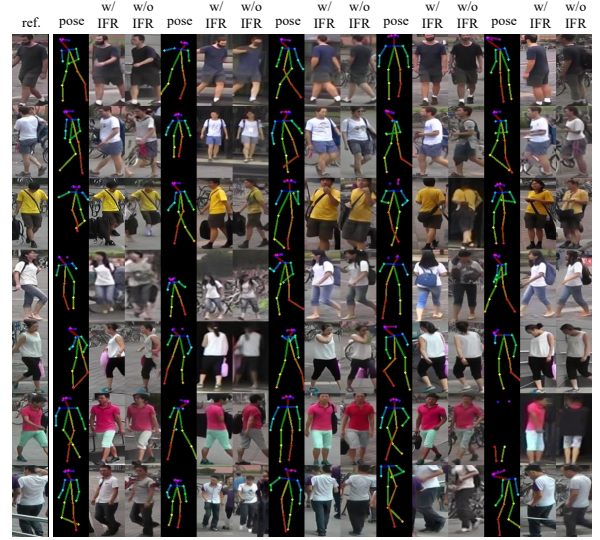


Figure 5. The effects with and without the IFR module were visualized with five different poses randomly selected for each reference picture.

N	Gallery ^{IPG}			Query ^{IPG}			Gallery ^{IPG} +Query ^{IPG}		
	mAP \uparrow	R1 \uparrow	ID $^2\downarrow$	mAP \uparrow	R1 \uparrow	ID $^2\downarrow$	mAP \uparrow	R1 \uparrow	ID $^2\downarrow$
0	79.88	91.48	0.2313	79.88	91.48	0.1623	79.88	91.48	0.2193
1	80.96	90.97	0.2087	79.99	90.83	0.1363	82.13	92.01	0.1961
2	82.86	91.45	0.1904	81.17	92.04	0.1156	85.27	93.71	0.1773
3	83.42	91.75	0.1837	81.55	92.25	0.1077	86.16	94.21	0.1704
4	83.81	92.1	0.1795	81.76	92.34	0.1027	86.75	94.24	0.1661
5	84.07	91.83	0.1758	81.85	92.07	0.0984	87.23	94.71	0.1623
6	84.3	91.98	0.1730	81.96	92.52	0.0950	87.52	94.63	0.1593
7	84.49	91.86	0.1707	82.03	92.37	0.0922	87.76	94.60	0.1570
8	84.65	92.07	0.1691	82.18	92.40	0.0902	88.02	94.77	0.1553

Table 6. Performance Comparison by adding numbers of generated images for each image on gallery, query, and both

Therefore, even if the features of an individual sample lack the pedestrian matching capability, as shown in the first row of Tab.5, its mAP and Rank-1 are only 3.34% and 11.4%. However, with our method, it improved 53.93%/70.99% to 57.27%/82.39%. Additionally, we visualized of 10 IDs' feature distributions using t-SNE as shown in Fig.4.

4.4. Abilation Study

Impact of the NFC and IPG. We conducted comprehensive ablation experiments on Neighbor Feature Centralization (NFC) and Feature ID-Centralizing through Identity-Guided Generation (IPG) methods. As shown in Table 2, 3, 4, which show great improvements.

Effect of Feature Re-Distribute Module. We randomly selected 7 images from the Market1501 dataset, choosing 5 different poses for each image. We visualized the results both with and without Identity Feature Redistribute (IFR)



Figure 6. Images generated with random poses. More randomly generated images can be found in Supplementary.

Module. As shown in Fig.5, the impact of ID features on the generated outcomes is evident.

Effect of numbers of generated images. We randomly selected different numbers of images generated from the 8 representative poses to verify the effect of feature enhancement. As shown in Tab.6, the experimental results align with the theory mentioned in Section3.1: the more features of the same ID that are aggregated, the more the adjustment noise extracted from individual images is reduced, enhancing the ID representation capability and resulting in improved matching performance.

4.5. Visualizations

Different people with the same poses across datasets. We are working on Market1501, SYSU-MM01, and Occluded-ReID datasets to visualize the 8 representative poses with only one model and results are shown in Fig.2.

Random people with random poses. To demonstrate the advancement of our model, as shown in Fig.6, we randomly chose samples from the whole dataset, and each sample ran-

domly chose poses, including some problematic poses, fully demonstrating the diversity of model. **More examples on three datasets are visualized in Supplementary.**

5. Conclusion

In this paper, we proposed a training-free person re-identification framework that fully leverages the natural clustering behavior of features around the identity center during the training process. By introducing the concept of feature centralization, we effectively reduced noise in individual samples and enhanced identity representation without model training. Our approach includes an identity-guided pedestrian generation paradigm, capable of producing high-quality, multi-pose images with consistent identity features, even under challenging conditions such as visible, infrared, and occlusion scenarios. The neighbor feature centralization algorithm also preserves feature’s original distribution while mining potential positive samples. It can also be flexibly integrated with existing re-ranking methods.

References

- [1] Jean-Paul Aïme, Ke Qin, Guisong Liu, and Guangchun Luo. Sparse label smoothing regularization for person re-identification. *IEEE Access*, 7:27899–27910, 2019. 3
- [2] Dosovitskiy Alexey. An image is worth 16x16 words: Transformers for image recognition at scale. *arXiv preprint arXiv:2010.11929*, 2020. 2
- [3] Sławomir Bak, Etienne Corvee, Francois Bremond, and Monique Thonnat. Person re-identification using haar-based and dcd-based signature. In *2010 7th IEEE international conference on advanced video and signal based surveillance*, pages 1–8. IEEE, 2010. 2
- [4] Ankan Kumar Bhunia, Salman Khan, Hisham Cholakkal, Rao Muhammad Anwer, Jorma Laaksonen, Mubarak Shah, and Fahad Shahbaz Khan. Person image synthesis via denoising diffusion model. In *Proceedings of the IEEE/CVF Conference on Computer Vision and Pattern Recognition*, pages 5968–5976, 2023. 3
- [5] Alessandro Borgia, Yang Hua, Elyor Kodirov, and Neil Robertson. Gan-based pose-aware regulation for video-based person re-identification. In *2019 IEEE Winter Conference on Applications of Computer Vision (WACV)*, pages 1175–1184. IEEE, 2019. 3
- [6] Weihua Chen, Xianzhe Xu, Jian Jia, Hao Luo, Yaohua Wang, Fan Wang, Rong Jin, and Xiuyu Sun. Beyond appearance: a semantic controllable self-supervised learning framework for human-centric visual tasks. In *Proceedings of the IEEE/CVF conference on computer vision and pattern recognition*, pages 15050–15061, 2023. 5
- [7] Pingyang Dai, Rongrong Ji, Haibin Wang, Qiong Wu, and Yuyu Huang. Cross-modality person re-identification with generative adversarial training. In *IJCAI*, page 6, 2018. 3
- [8] Chanhoe Eom and Bumsu Ham. Learning disentangled representation for robust person re-identification. *Advances in neural information processing systems*, 32, 2019. 3
- [9] Xingye Fang, Yang Yang, and Ying Fu. Visible-infrared person re-identification via semantic alignment and affinity inference. In *Proceedings of the IEEE/CVF International Conference on Computer Vision*, pages 11270–11279, 2023. 6
- [10] Jiawei Feng, Ancong Wu, and Wei-Shi Zheng. Shape-erased feature learning for visible-infrared person re-identification. In *Proceedings of the IEEE/CVF Conference on Computer Vision and Pattern Recognition*, pages 22752–22761, 2023. 6
- [11] Dengpan Fu, Dongdong Chen, Jianmin Bao, Hao Yang, Lu Yuan, Lei Zhang, Houqiang Li, and Dong Chen. Unsupervised pre-training for person re-identification. In *Proceedings of the IEEE/CVF conference on computer vision and pattern recognition*, pages 14750–14759, 2021. 2
- [12] Shang Gao, Jingya Wang, Huchuan Lu, and Zimo Liu. Pose-guided visible part matching for occluded person reid. In *Proceedings of the IEEE/CVF conference on computer vision and pattern recognition*, pages 11744–11752, 2020. 5
- [13] Yixiao Ge, Zhuowan Li, Haiyu Zhao, Guojun Yin, Shuai Yi, Xiaogang Wang, et al. Fd-gan: Pose-guided feature distilling gan for robust person re-identification. *Advances in neural information processing systems*, 31, 2018. 2
- [14] Ian Goodfellow, Jean Pouget-Abadie, Mehdi Mirza, Bing Xu, David Warde-Farley, Sherjil Ozair, Aaron Courville, and Yoshua Bengio. Generative adversarial nets. *Advances in neural information processing systems*, 27, 2014. 3
- [15] Xin Hao, Sanyuan Zhao, Mang Ye, and Jianbing Shen. Cross-modality person re-identification via modality confusion and center aggregation. In *Proceedings of the IEEE/CVF International Conference on Computer Vision*, pages 16403–16412, 2021. 6
- [16] Shutong He, Hao Luo, Pichao Wang, Fan Wang, Hao Li, and Wei Jiang. Transreid: Transformer-based object re-identification. In *Proceedings of the IEEE/CVF international conference on computer vision*, pages 15013–15022, 2021. 6, 7, 5
- [17] Alexander Hermans, Lucas Beyer, and Bastian Leibe. In defense of the triplet loss for person re-identification. *arXiv preprint arXiv:1703.07737*, 2017. 2
- [18] Martin Hirzer, Peter M Roth, Martin Köstinger, and Horst Bischof. Relaxed pairwise learned metric for person re-identification. In *Computer Vision—ECCV 2012: 12th European Conference on Computer Vision, Florence, Italy, October 7–13, 2012, Proceedings, Part VI 12*, pages 780–793. Springer, 2012. 2
- [19] Jonathan Ho, Ajay Jain, and Pieter Abbeel. Denoising diffusion probabilistic models. *Advances in neural information processing systems*, 33:6840–6851, 2020. 2, 3
- [20] Li Hu. Animate anyone: Consistent and controllable image-to-video synthesis for character animation. In *Proceedings of the IEEE/CVF Conference on Computer Vision and Pattern Recognition*, pages 8153–8163, 2024. 5
- [21] Yan Huang, Qiang Wu, Jingsong Xu, and Yi Zhong. Sbagan: Suppression of inter-domain background shift for person re-identification. In *Proceedings of the IEEE/CVF International Conference on Computer Vision*, pages 9527–9536, 2019. 3
- [22] Zhipeng Huang, Jiawei Liu, Liang Li, Kecheng Zheng, and Zhengjun Zha. Modality-adaptive mixup and invariant decomposition for rgb-infrared person re-identification. In *AAAI Conference on Artificial Intelligence*, 2022. 6
- [23] Saleh Hussin Salem Hussin and Remzi Yildirim. Stylegan-lsro method for person re-identification. *IEEE Access*, 9: 13857–13869, 2021. 3
- [24] Kongzhu Jiang, Tianzhu Zhang, Xiang Liu, Bingqiao Qian, Yongdong Zhang, and Feng Wu. Cross-modality transformer for visible-infrared person re-identification. In *European Conference on Computer Vision*, pages 480–496. Springer, 2022. 6
- [25] Minsu Kim, Seungryong Kim, Jungin Park, Seongheon Park, and Kwanghoon Sohn. Partmix: Regularization strategy to learn part discovery for visible-infrared person re-identification. In *Proceedings of the IEEE/CVF Conference on Computer Vision and Pattern Recognition*, pages 18621–18632, 2023. 6
- [26] Diederik P Kingma. Auto-encoding variational bayes. *arXiv preprint arXiv:1312.6114*, 2013. 5, 7
- [27] Diederik P Kingma. Adam: A method for stochastic optimization. *arXiv preprint arXiv:1412.6980*, 2014. 7
- [28] Martin Koestinger, Martin Hirzer, Paul Wohlhart, Peter M Roth, and Horst Bischof. Large scale metric learning from

- equivalence constraints. In *2012 IEEE conference on computer vision and pattern recognition*, pages 2288–2295. IEEE, 2012. 2
- [29] Alex Krizhevsky, Ilya Sutskever, and Geoffrey E Hinton. Imagenet classification with deep convolutional neural networks. *Advances in neural information processing systems*, 25, 2012. 2
- [30] Ryan Layne, Timothy M Hospedales, Shaogang Gong, and Q Mary. Person re-identification by attributes. In *Bmvc*, page 8, 2012. 2
- [31] Siyuan Li, Li Sun, and Qingli Li. Clip-reid: exploiting vision-language model for image re-identification without concrete text labels. In *Proceedings of the AAAI Conference on Artificial Intelligence*, pages 1405–1413, 2023. 6, 5
- [32] Xulin Li, Yan Lu, Bin Liu, Yating Liu, Guojun Yin, Qi Chu, Jinyang Huang, Feng Zhu, Rui Zhao, and Nenghai Yu. Counterfactual intervention feature transfer for visible-infrared person re-identification. In *European conference on computer vision*, pages 381–398. Springer, 2022. 6
- [33] Yulin Li, Jianfeng He, Tianzhu Zhang, Xiang Liu, Yongdong Zhang, and Feng Wu. Diverse part discovery: Occluded person re-identification with part-aware transformer. In *Proceedings of the IEEE/CVF conference on computer vision and pattern recognition*, pages 2898–2907, 2021. 5
- [34] Shengcai Liao and Stan Z Li. Efficient psd constrained asymmetric metric learning for person re-identification. In *Proceedings of the IEEE international conference on computer vision*, pages 3685–3693, 2015. 2
- [35] Shengcai Liao and Ling Shao. Interpretable and generalizable person re-identification with query-adaptive convolution and temporal lifting. In *Computer Vision—ECCV 2020: 16th European Conference, Glasgow, UK, August 23–28, 2020, Proceedings, Part XI 16*, pages 456–474. Springer, 2020. 2
- [36] Jinxian Liu, Bingbing Ni, Yichao Yan, Peng Zhou, Shuo Cheng, and Jianguo Hu. Pose transferrable person re-identification. In *Proceedings of the IEEE conference on computer vision and pattern recognition*, pages 4099–4108, 2018. 3
- [37] Jialun Liu, Yifan Sun, Feng Zhu, Hongbin Pei, Yi Yang, and Wenhui Li. Learning memory-augmented unidirectional metrics for cross-modality person re-identification. *2022 IEEE/CVF Conference on Computer Vision and Pattern Recognition (CVPR)*, pages 19344–19353, 2022. 6
- [38] Hu Lu, Xuezhong Zou, and Pingping Zhang. Learning progressive modality-shared transformers for effective visible-infrared person re-identification. In *Proceedings of the AAAI conference on artificial intelligence*, pages 1835–1843, 2023. 6
- [39] Hao Luo, Youzhi Gu, Xingyu Liao, Shenqi Lai, and Wei Jiang. Bag of tricks and a strong baseline for deep person re-identification. In *Proceedings of the IEEE/CVF conference on computer vision and pattern recognition workshops*, pages 0–0, 2019. 5
- [40] Fei Ma, Xiao-Yuan Jing, Xiao Zhu, Zhenmin Tang, and Zhiping Peng. True-color and grayscale video person re-identification. *IEEE Transactions on Information Forensics and Security*, 15:115–129, 2019. 2
- [41] Niall McLaughlin, Jesus Martinez Del Rincon, and Paul Miller. Data-augmentation for reducing dataset bias in person re-identification. In *2015 12th IEEE International conference on advanced video and signal based surveillance (AVSS)*, pages 1–6. IEEE, 2015. 2
- [42] Zhiqi Pang, Jifeng Guo, Wenbo Sun, Yanbang Xiao, and Ming Yu. Cross-domain person re-identification by hybrid supervised and unsupervised learning. *Applied Intelligence*, 52(3):2987–3001, 2022. 3
- [43] Xuelin Qian, Yanwei Fu, Tao Xiang, Wenxuan Wang, Jie Qiu, Yang Wu, Yu-Gang Jiang, and Xiangyang Xue. Pose-normalized image generation for person re-identification. In *Proceedings of the European conference on computer vision (ECCV)*, pages 650–667, 2018. 2, 3
- [44] Robin Rombach, Andreas Blattmann, Dominik Lorenz, Patrick Esser, and Björn Ommer. High-resolution image synthesis with latent diffusion models. In *Proceedings of the IEEE/CVF conference on computer vision and pattern recognition*, pages 10684–10695, 2022. 3, 4, 6
- [45] Aliaksandr Siarohin, Enver Sangineto, Stéphane Lathuilière, and Nicu Sebe. Deformable gans for pose-based human image generation. In *Proceedings of the IEEE conference on computer vision and pattern recognition*, pages 3408–3416, 2018. 3
- [46] Vladimir Somers, Christophe De Vleeschouwer, and Alexandre Alahi. Body part-based representation learning for occluded person re-identification. In *Proceedings of the IEEE/CVF winter conference on applications of computer vision*, pages 1613–1623, 2023. 6, 5
- [47] Vladimir Somers, Alexandre Alahi, and Christophe De Vleeschouwer. Keypoint promptable re-identification. In *European Conference on Computer Vision*, pages 216–233. Springer, 2025. 6, 5
- [48] Yifan Sun, Liang Zheng, Weijian Deng, and Shengjin Wang. Svdnet for pedestrian retrieval. In *Proceedings of the IEEE international conference on computer vision*, pages 3800–3808, 2017. 2
- [49] Yifan Sun, Liang Zheng, Yi Yang, Qi Tian, and Shengjin Wang. Beyond part models: Person retrieval with refined part pooling (and a strong convolutional baseline). In *Proceedings of the European conference on computer vision (ECCV)*, pages 480–496, 2018. 5
- [50] Christian Szegedy, Vincent Vanhoucke, Sergey Ioffe, Jon Shlens, and Zbigniew Wojna. Rethinking the inception architecture for computer vision. In *Proceedings of the IEEE conference on computer vision and pattern recognition*, pages 2818–2826, 2016. 3
- [51] Guan'an Wang, Shuo Yang, Huanyu Liu, Zhicheng Wang, Yang Yang, Shuliang Wang, Gang Yu, Erjin Zhou, and Jian Sun. High-order information matters: Learning relation and topology for occluded person re-identification. In *Proceedings of the IEEE/CVF conference on computer vision and pattern recognition*, pages 6449–6458, 2020. 5
- [52] Tao Wang, Hong Liu, Pinhao Song, Tianyu Guo, and Wei Shi. Pose-guided feature disentangling for occluded person re-identification based on transformer. In *Proceedings of the AAAI conference on artificial intelligence*, pages 2540–2549, 2022. 5

- [53] Zhikang Wang, Feng Zhu, Shixiang Tang, Rui Zhao, Lihuo He, and Jiangning Song. Feature erasing and diffusion network for occluded person re-identification. In *Proceedings of the IEEE/CVF conference on computer vision and pattern recognition*, pages 4754–4763, 2022. 5
- [54] Longhui Wei, Shiliang Zhang, Wen Gao, and Qi Tian. Person transfer gan to bridge domain gap for person re-identification. In *Proceedings of the IEEE conference on computer vision and pattern recognition*, pages 79–88, 2018. 7
- [55] Ancong Wu, Wei-Shi Zheng, Hong-Xing Yu, Shaogang Gong, and Jianhuang Lai. Rgb-infrared cross-modality person re-identification. In *Proceedings of the IEEE international conference on computer vision*, pages 5380–5389, 2017. 2, 7
- [56] Jianbing Wu, Hong Liu, Yuxin Su, Wei Shi, and Hao Tang. Learning concordant attention via target-aware alignment for visible-infrared person re-identification. In *2023 IEEE/CVF International Conference on Computer Vision (ICCV)*, pages 11088–11097, 2023. 6
- [57] Qiong Wu, Pingyang Dai, Jie Chen, Chia-Wen Lin, Yongjian Wu, Feiyue Huang, Bineng Zhong, and Rongrong Ji. Discover cross-modality nuances for visible-infrared person re-identification. In *Proceedings of the IEEE/CVF conference on computer vision and pattern recognition*, pages 4330–4339, 2021. 6
- [58] Cheng Yan, Guansong Pang, Jile Jiao, Xiao Bai, Xuetao Feng, and Chunhua Shen. Occluded person re-identification with single-scale global representations. In *Proceedings of the IEEE/CVF international conference on computer vision*, pages 11875–11884, 2021. 5
- [59] Jinrui Yang, Jiawei Zhang, Fufu Yu, Xinyang Jiang, Mengdan Zhang, Xing Sun, Ying-Cong Chen, and Wei-Shi Zheng. Learning to know where to see: A visibility-aware approach for occluded person re-identification. In *Proceedings of the IEEE/CVF international conference on computer vision*, pages 11885–11894, 2021. 5
- [60] Zhenhong Yang, Ailing Zeng, Chun Yuan, and Yu Li. Effective whole-body pose estimation with two-stages distillation. In *Proceedings of the IEEE/CVF International Conference on Computer Vision*, pages 4210–4220, 2023. 3
- [61] Hao Yu, Xu Cheng, Wei Peng, Weihao Liu, and Guoying Zhao. Modality unifying network for visible-infrared person re-identification. In *Proceedings of the IEEE/CVF International Conference on Computer Vision*, pages 11185–11195, 2023. 6
- [62] Hong-Xing Yu, Ancong Wu, and Wei-Shi Zheng. Unsupervised person re-identification by deep asymmetric metric embedding. *IEEE transactions on pattern analysis and machine intelligence*, 42(4):956–973, 2018. 2
- [63] Chengyuan Zhang, Lei Zhu, ShiChao Zhang, and Weiren Yu. Pac-gan: An effective pose augmentation scheme for unsupervised cross-view person re-identification. *Neurocomputing*, 387:22–39, 2020. 3
- [64] Guiwei Zhang, Yongfei Zhang, and Zichang Tan. Protohpe: Prototype-guided high-frequency patch enhancement for visible-infrared person re-identification. In *Proceedings of the 31st ACM International Conference on Multimedia*, pages 944–954, 2023. 2, 6
- [65] Guiwei Zhang, Yongfei Zhang, Tianyu Zhang, Bo Li, and Shiliang Pu. Pha: Patch-wise high-frequency augmentation for transformer-based person re-identification. In *Proceedings of the IEEE/CVF conference on computer vision and pattern recognition*, pages 14133–14142, 2023. 2
- [66] Lvmin Zhang, Anyi Rao, and Maneesh Agrawala. Adding conditional control to text-to-image diffusion models. In *Proceedings of the IEEE/CVF International Conference on Computer Vision*, pages 3836–3847, 2023. 2, 3
- [67] Qiang Zhang, Changzhou Lai, Jianan Liu, Nianchang Huang, and Jungong Han. Fmcnet: Feature-level modality compensation for visible-infrared person re-identification. In *Proceedings of the IEEE/CVF Conference on Computer Vision and Pattern Recognition*, pages 7349–7358, 2022. 6
- [68] Yukang Zhang and Hanzi Wang. Diverse embedding expansion network and low-light cross-modality benchmark for visible-infrared person re-identification. In *Proceedings of the IEEE/CVF conference on computer vision and pattern recognition*, pages 2153–2162, 2023. 6
- [69] Yiyuan Zhang, Sanyuan Zhao, Yuhao Kang, and Jianbing Shen. Modality synergy complement learning with cascaded aggregation for visible-infrared person re-identification. In *European Conference on Computer Vision*, pages 462–479. Springer, 2022. 6
- [70] Liang Zheng, Liyue Shen, Lu Tian, Shengjin Wang, Jingdong Wang, and Qi Tian. Scalable person re-identification: A benchmark. In *Proceedings of the IEEE international conference on computer vision*, pages 1116–1124, 2015. 2, 7
- [71] Liang Zheng, Zhi Bie, Yifan Sun, Jingdong Wang, Chi Su, Shengjin Wang, and Qi Tian. Mars: A video benchmark for large-scale person re-identification. In *Computer Vision—ECCV 2016: 14th European Conference, Amsterdam, The Netherlands, October 11–14, 2016, Proceedings, Part VI 14*, pages 868–884. Springer, 2016. 7
- [72] Zhenhong Zheng, Liang Zheng, and Yi Yang. Unlabeled samples generated by gan improve the person re-identification baseline in vitro. In *Proceedings of the IEEE international conference on computer vision*, pages 3754–3762, 2017. 2, 3, 5
- [73] Zhenhong Zheng, Xiaodong Yang, Zhiding Yu, Liang Zheng, Yi Yang, and Jan Kautz. Joint discriminative and generative learning for person re-identification. In *proceedings of the IEEE/CVF conference on computer vision and pattern recognition*, pages 2138–2147, 2019. 2, 3
- [74] Zhun Zhong, Liang Zheng, Donglin Cao, and Shaozi Li. Re-ranking person re-identification with k-reciprocal encoding. In *Proceedings of the IEEE conference on computer vision and pattern recognition*, pages 1318–1327, 2017. 2, 3
- [75] Zhun Zhong, Liang Zheng, Zhenhong Zheng, Shaozi Li, and Yi Yang. Camstyle: A novel data augmentation method for person re-identification. *IEEE Transactions on Image Processing*, 28(3):1176–1190, 2018. 3
- [76] Zhun Zhong, Liang Zheng, Guoliang Kang, Shaozi Li, and Yi Yang. Random erasing data augmentation. In *Proceedings of the AAAI conference on artificial intelligence*, pages 13001–13008, 2020. 2, 7

- [77] Kuan Zhu, Haiyun Guo, Zhiwei Liu, Ming Tang, and Jinqiao Wang. Identity-guided human semantic parsing for person re-identification. In *Computer Vision—ECCV 2020: 16th European Conference, Glasgow, UK, August 23–28, 2020, Proceedings, Part III 16*, pages 346–363. Springer, 2020. [5](#)
- [78] Jiaxuan Zhuo, Zeyu Chen, Jianhuang Lai, and Guangcong Wang. Occluded person re-identification. In *2018 IEEE international conference on multimedia and expo (ICME)*, pages 1–6. IEEE, 2018. [2](#)

From Poses to Identity: Training-Free Person Re-Identification via Feature Centralization

Supplementary Material

6. Methods Supplementary

6.1. Aggregation role of ReID loss functions

Currently, ReID models commonly use cross-entropy loss to impose ID-level constraints, and contrastive losses (such as triplet loss) to bring features of the same ID closer while pushing apart features of different IDs. Some models also utilize center loss to construct identity centers for dynamically constraining the IDs. These methods lead to one common result: feature aggregation. From the perspective of the gradient of the loss functions, we could prove that the feature vectors of each ID in current ReID tasks naturally aggregate around a center or mean in the followings.

Cross-Entropy Loss is often used in classification tasks, optimizing the model by maximizing the probability of the correct class. Given N samples, each with a feature vector $\mathbf{z}_i \in \mathbb{R}^d$, and its corresponding class label $y_i \in \{1, 2, \dots, C\}$, the cross-entropy loss is defined as:

$$\mathcal{L}_{\text{CE}} = -\frac{1}{N} \sum_{i=1}^N \log \frac{\exp(\mathbf{w}_{y_i}^\top \mathbf{z}_i + b_{y_i})}{\sum_{j=1}^C \exp(\mathbf{w}_j^\top \mathbf{z}_i + b_j)} \quad (10)$$

where \mathbf{w}_j and b_j are the weight vector and bias for class j , respectively.

For simplicity, assume that the final layer is a linear classifier without bias, i.e., $b_j = 0$. When the loss is minimized, the optimization objective is to maximize the score $\mathbf{w}_{y_i}^\top \mathbf{z}_i$ of the correct class while minimizing the scores $\mathbf{w}_j^\top \mathbf{z}_i$ of other classes ($j \neq y_i$).

By gradient descent optimization, we can obtain:

$$\frac{\partial \mathcal{L}_{\text{CE}}}{\partial \mathbf{z}_i} = 1/N (p_{y_i} - 1) \mathbf{w}_{y_i} + 1/N \sum_{j \neq y_i} p_{ij} \mathbf{w}_j \quad (11)$$

where $p_{ij} = \frac{\exp(\mathbf{w}_j^\top \mathbf{z}_i)}{\sum_{k=1}^C \exp(\mathbf{w}_k^\top \mathbf{z}_i)}$.

With the loss function converges, $p_{y_i} \rightarrow 1$ and $p_{ij} \rightarrow 0 (j \neq y_i)$. The feature \mathbf{z}_i is optimized to be near a linear combination of the class weight vectors \mathbf{w}_{y_i} . This indicates that features of the same class will tend toward a common direction, thus achieving feature aggregation.

Contrastive loss (Triplet Loss as example) optimizes the feature space by bringing samples of the same class closer and pushing samples of different classes further apart. A triplet $(\mathbf{z}_a, \mathbf{z}_p, \mathbf{z}_n)$ is defined, where \mathbf{z}_a is the anchor, \mathbf{z}_p

is the positive sample (same class), and \mathbf{z}_n is the negative sample (different class). The triplet loss is defined as:

$$\mathcal{L}_{\text{Triplet}} = \max(\|\mathbf{z}_a - \mathbf{z}_p\|_2^2 - \|\mathbf{z}_a - \mathbf{z}_n\|_2^2 + \alpha, 0) \quad (12)$$

where α is the margin parameter.

To minimize the loss, the optimization objective is:

$$\|\mathbf{z}_a - \mathbf{z}_p\|_2^2 + \alpha < \|\mathbf{z}_a - \mathbf{z}_n\|_2^2 \quad (13)$$

$$\frac{\partial \mathcal{L}_{\text{Triplet}}}{\partial \mathbf{z}_a} = 2(\mathbf{z}_n - \mathbf{z}_p), \quad (14)$$

$$\frac{\partial \mathcal{L}_{\text{Triplet}}}{\partial \mathbf{z}_p} = 2(\mathbf{z}_p - \mathbf{z}_a), \quad (15)$$

$$\frac{\partial \mathcal{L}_{\text{Triplet}}}{\partial \mathbf{z}_n} = 2(\mathbf{z}_a - \mathbf{z}_n). \quad (16)$$

By minimizing triplet loss, the feature \mathbf{z}_p is pulled closer to \mathbf{z}_a , while \mathbf{z}_n is pushed away. Through this mechanism, Triplet Loss encourages features of the same class to aggregate together while features of different classes are separated from each other.

Center loss further enhances feature aggregation by introducing a feature center for each class. For each class j , there is a feature center \mathbf{c}_j , and the center loss is defined as:

$$\mathcal{L}_{\text{Center}} = \frac{1}{2} \sum_{i=1}^N \|\mathbf{z}_i - \mathbf{c}_{y_i}\|_2^2 \quad (17)$$

The goal of minimizing center loss is to make each sample's feature vector \mathbf{z}_i as close as possible to its corresponding class center \mathbf{c}_{y_i} . Through gradient descent, we obtain:

$$\frac{\partial \mathcal{L}_{\text{Center}}}{\partial \mathbf{z}_i} = \mathbf{z}_i - \mathbf{c}_{y_i} \quad (18)$$

$$\frac{\partial \mathcal{L}_{\text{Center}}}{\partial \mathbf{c}_j} = \begin{cases} \mathbf{c}_j - \mathbf{z}_i & \text{if } y_i = j \\ 0 & \text{otherwise} \end{cases} \quad (19)$$

Thus, the optimization process not only pulls sample features closer to their centers but also dynamically updates each class's center to represent the mean of that class's feature distribution. This directly encourages features of the same class to aggregate together.

6.2. Identity Density (ID²) Metric

Identity density is one aspect of measuring ReID effectiveness. However, there is currently no quantitative metric for this, and researchers commonly rely on visualization tools like t-SNE to demonstrate model performance. Due to the large number of IDs, this approach is limited to visualizing only a few IDs, making it challenging to assess model performance from a global perspective quantitatively. Some researchers exploit this limitation by selecting the best-performing IDs of their models for visualization. To address this, we propose an Identity Density (ID²) Metric. This metric evaluates the global ID aggregation performance by taking each ID center across the entire test set (gallery and query) as a benchmark.

$$\text{ID}^2 = \frac{1}{N} \sum_{i=1}^N \frac{1}{n_i} \sum_{j=1}^{n_i} d\left(\frac{f_{ij}}{\|f_{ij}\|_2}, c_i\right) \quad (20)$$

where N is the total number of unique IDs in the test set, and n_i is the number of samples for ID i . The feature vector of the j -th sample of ID i is denoted as f_{ij} , and c_i represents the identity center of ID i , computed as follows:

$$c_i = \frac{1}{n_i} \sum_{j=1}^{n_i} \frac{f_{ij}}{\|f_{ij}\|_2} \quad (21)$$

Both the feature vectors f_{ij} and the identity centers c_i are L_2 -normalized to ensure consistent feature scaling. The function $d(\cdot, \cdot)$ represents the Euclidean distance.

6.3. Pose Encoder Details

The Pose Encoder module is designed to extract high-dimensional pose embeddings from the input poses.

$$\mathbf{E}_{\text{pose}} = \text{PoseEncoder}(\mathbf{x}^{\text{pose}}) \quad (22)$$

The input is a feature map of size $C_{\text{in}} \times H \times W$, denoted as \mathbf{x}^{pose} , where C_{in} is the number of input channels, and H, W are the height, and width of the input. The first convolution layer is defined as:

$$\mathbf{E}_0 = \text{SiLU}(\text{Conv}_{\text{in}}(\mathbf{x}^{\text{pose}})) \quad (23)$$

where Conv_{in} is a convolution operation with kernel size 3×3 , and the number of channels changes from $C_{\text{in}} = 3$ to $C_0 = 16$:

Each block applies a normal 3×3 Conv, a 3×3 Conv with stride 2 to reduce spatial dimensions, and followed by a SiLU activate function. For the i -th convolutional block, the operations can be expressed as:

$$\mathbf{E}_{i+1} = \text{SiLU}(\text{Conv}_{i, \text{stride}=2}(\text{Conv}_i(\mathbf{E}_i))) \quad (24)$$

The number of channels for each block is as follows: $[C_0, C_1, C_2, C_3] = [16, 32, 64, 128]$

The output Conv layer maps the features from the last block to the target embedding dimension $C_{\text{out}} = 320$, expressed as:

$$\mathbf{E}_{\text{pose}} = \text{Conv}_{\text{out}}(\mathbf{E}_4) \quad (25)$$

6.4. Detailed Description of Neighbor Feature Centralization (NFC)

Step 1: Compute Distance Matrix Given all feature vectors in the gallery $\{\mathbf{z}_i\}_{i=1}^N$, our goal is to enhance each feature vector by aggregating features from its mutual nearest neighbors. Compute the pairwise distance matrix $\mathbf{D} = [d_{ij}]$ where d_{ij} represents the distance between features \mathbf{z}_i and \mathbf{z}_j . To avoid self-matching, set the diagonal elements to a large constant, i.e.

$$d_{ii} = C, \quad \text{for } i = 1, 2, \dots, N$$

Step 2: Find Top k_1 Nearest Neighbors For each feature \mathbf{z}_i , find its top k_1 nearest neighbors based on the distance matrix \mathbf{D} . Denote the set of indices of these neighbors as:

$$\mathcal{N}_i = \text{TopK}_{k_1}(\{d_{ij}\}_{j=1}^N) \quad (26)$$

Step 3: Identify Mutual Nearest Neighbors For each feature \mathbf{z}_i , identifies its mutual nearest neighbors by checking whether each neighbor in \mathcal{N}_i also considers \mathbf{z}_i as one of its top k_2 nearest neighbors. Specifically, for each $j \in \mathcal{N}_i$, checks if $i \in \mathcal{N}_j^{k_2}$, where $\mathcal{N}_j^{k_2}$ is the set of indices of the top k_2 nearest neighbors of \mathbf{z}_j . If this condition is satisfied, add j to the mutual nearest neighbor set \mathcal{M}_i :

$$\mathcal{M}_i = \{j \mid j \in \mathcal{N}_i, i \in \mathcal{N}_j^{k_2}\} \quad (27)$$

Step 4: Feature Centralization Enhancement Then it could centralize each feature vector \mathbf{z}_i by aggregating the features of its mutual nearest neighbors:

$$\mathbf{z}_i^{\text{centralized}} = \mathbf{z}_i + \sum_{j \in \mathcal{M}_i} \mathbf{z}_j \quad (28)$$

This aggregation reduces feature noise and improves discriminability by incorporating information from similar features.

7. Experiments Supplementary

7.1. Data Cleansing

Training an effective generative model requires high-quality data support. In current ReID (Person Re-Identification) datasets, there are many low-quality images, and removing them can help reduce interference to the model. In our experiments, we found two main issues that need to be addressed: **Extremely Low-quality Images**: The dataset contains images with such low resolution that even the human

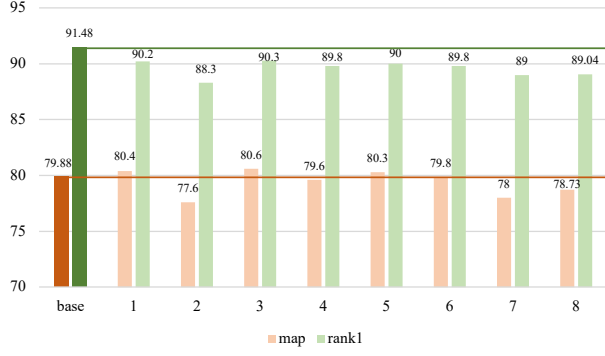


Figure 7. ReID results with images generated with the same pose on Market1501.

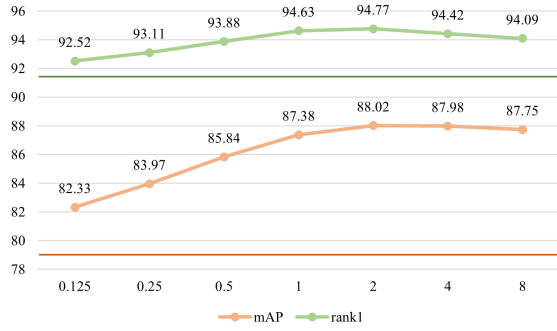


Figure 8. Impact of the quality coefficient η with TransReID on Market1501. The dark color lines are the baseline.

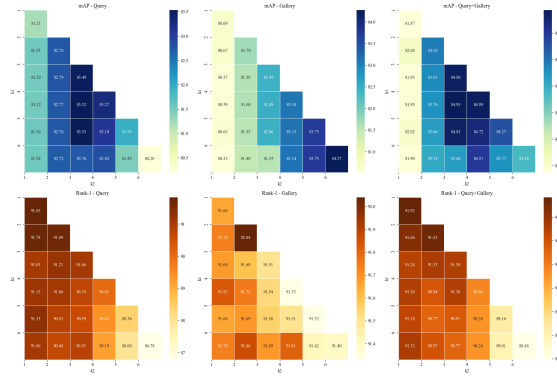


Figure 9. k_1/k_2 analysis of Neighbor Feature Centralization (NFC) with TransReID on Market1501 without re-ranking.

eye cannot recognize them as a "person". **Pose Estimation Failures:** The pose estimation model inevitably fails to detect pedestrian poses in some images.

7.1.1. Extremely Low-quality Images

To address this, manual filtering is impractical. Therefore, we designed an automated filtering algorithm. We leverage normal distribution of feature vector, if the feature on the

edge of the distribution, largely due to the data itself is out of the distribution of its identity, and it can be picked up.

Let $\mathbf{f}_i \in \mathbb{R}^d$ denote the feature vector of the i -th sample of a particular identity, where d is the feature dimension. The mean vector $\boldsymbol{\mu}$ and covariance matrix $\boldsymbol{\Sigma}$ are computed as follows:

$$\boldsymbol{\mu} = \frac{1}{N} \sum_{i=1}^N \mathbf{f}_i, \quad \boldsymbol{\Sigma} = \frac{1}{N} \sum_{i=1}^N (\mathbf{f}_i - \boldsymbol{\mu})(\mathbf{f}_i - \boldsymbol{\mu})^\top \quad (29)$$

where N is the number of samples for a given ID.

To detect outliers, we compute the Mahalanobis distance d_i of each feature vector \mathbf{f}_i from the mean vector $\boldsymbol{\mu}$, defined as:

$$dis_i = \sqrt{(\mathbf{f}_i - \boldsymbol{\mu})^\top \boldsymbol{\Sigma}^{-1} (\mathbf{f}_i - \boldsymbol{\mu})} \quad (30)$$

Given that the feature vectors are assumed to follow a multivariate normal distribution, we use quantiles of the Mahalanobis distance to filter out outliers. Specifically, we define a lower bound Q_p and an upper bound Q_{1-p} based on the p -th and $(1-p)$ -th quantiles, respectively. Samples with distances outside this range are considered outliers and are removed, and can get a set S_i^{ref} for i^{th} ID:

$$S_i^{\text{ref}} = \{\mathbf{x}_i \mid dis_i \in [Q_p, Q_{1-p}]\} \quad (31)$$

7.1.2. Pose Filtering for 'Failed' Pose Estimation

We designed a pose filtering algorithm called PoseValid to eliminate cases where pose extraction has "completely failed." This algorithm checks the validity of the pose keypoints based on factors such as occlusion, keypoint positions, angles, and limb proportions, then get the set of valid poses.

$$S_i^{\text{trg}} = \{\mathbf{x}_i \mid \text{PoseValid}(\mathbf{x}_i) \text{ and } dis_i \in [Q_p, Q_{1-p}]\} \quad (32)$$

where the pose detector in this paper uses pretrained model of DWpose[60]. Given a set of keypoints representing a pose, we normalize the pose using the following steps:

1. Compute the body height (h):
Calculate the Euclidean distance between the Neck (keypoint 1) and the Left Hip (keypoint 11):

$$h = \|\mathbf{k}_{\text{Neck}} - \mathbf{k}_{\text{LHip}}\|$$

2. Translate the pose:
Shift all keypoints so that the Neck is at the origin:

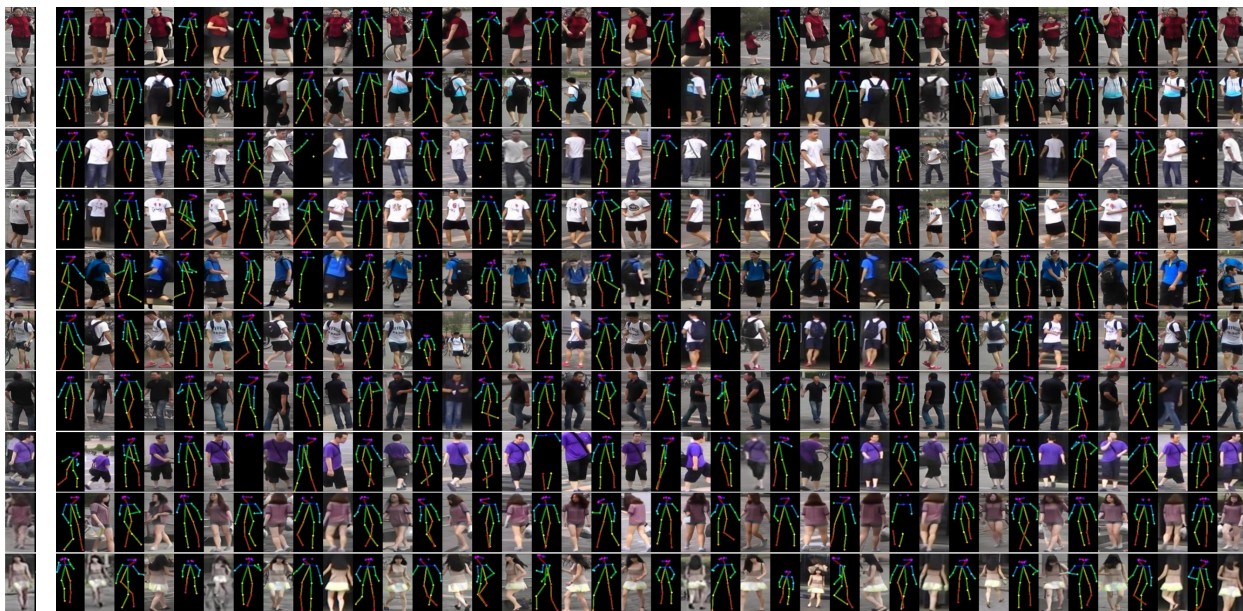
$$\mathbf{k}'_i = \mathbf{k}_i - \mathbf{k}_{\text{Neck}}$$

3. Scale the pose:
Divide each keypoint by the body height to normalize the size:

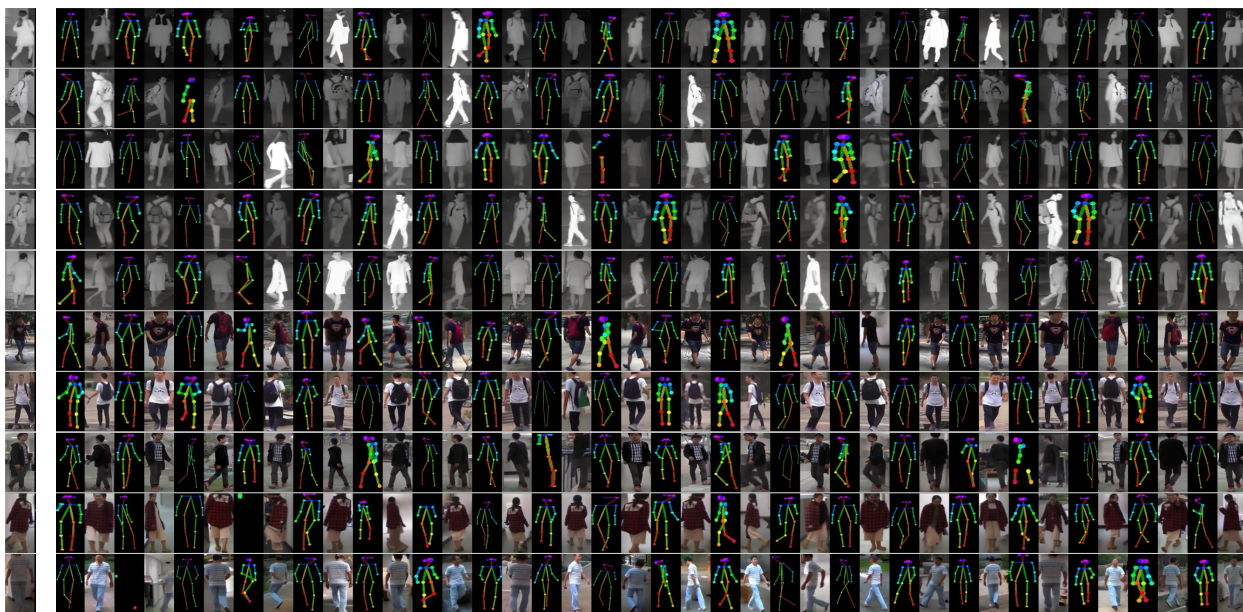
$$\mathbf{k}_i^{\text{normalized}} = \frac{\mathbf{k}'_i}{h}$$

Then, the filtering process of PoseValid function evaluates the validity of pose keypoints by applying constraints on limb lengths, symmetry, and keypoint positions.

Market1501



SYSU-MM01



Occluded-ReID

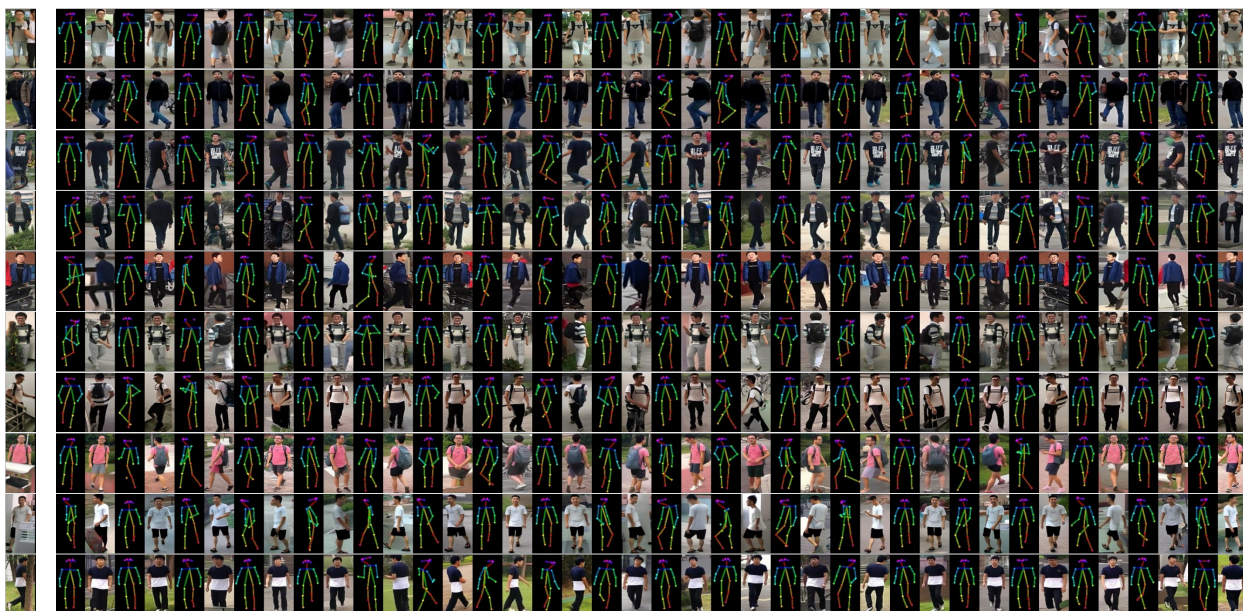


Figure 10. More random generated images on three datasets.



Figure 11. Some outliers detected via the mechanism formulated as Equation.31 on Market1501 and SYSU-MM01 with quartile 0.005.

+Ours	+Rerank	mAP	Rank1
✗	✗	79.88	91.48
✗	✓	89.56	92.07
✓	✗	90.39	94.74
✓	✓	92.79	94.83

Table 7. Compared to k-reciprocal rerank with official settings on Market1501 ($k_1=20, k_2=6$).

Methods	mAP	Rank1
TransReID on MSMT17	67.80	85.33
+ours	74.06	86.55

Table 8. Experiment on MSMT17 with TransReID and their official weights.

7.2. Generation quality and Pose Representation Study

To assess the quality of the generated images, we replaced the real images in the dataset with images of the same pose and performed inference validation. The results, as shown in Fig.7, indicate that the original model still successfully matches pedestrians without significant performance degradation. Even with all images in the same pose, the model can effectively differentiate between individuals. This suggests that our generated images are of high quality, retaining the main characteristics of the original images without notably impacting the ReID model. Moreover, we found that pedestrians walking at an angle have higher distinguishability compared to other poses (front, back, and side views), which are more representative of their identities.

7.3. More Random Generation

We provide additional randomly generated images in Fig.10 from Market-1501, SYSU-MM01 and Occluded-ReID datasets.

Methods	Market1501		Occluded-reID	
	Rank-1	mAP	Rank-1	mAP
BoT[39]	94.5	85.9	58.4	52.3
PCB[49]	93.8	81.6	-	-
VGTri[59]	-	-	81.0	71.0
PVPM[12]	-	-	66.8	59.5
HOReID[51]	94.2	84.9	80.3	70.2
ISP[77]	95.3	88.6	-	-
PAT[33]	95.4	88.0	81.6	72.1
TRANS[16]	95.2	88.9	-	-
CLIP[31]	95.7	89.8	-	-
SOLIDER[6]	96.9	93.9	-	-
SSGR[58]	96.1	89.3	78.5	72.9
FED[53]	95.0	86.3	86.3	79.3
BPBReid[46]	95.7	89.4	82.9	75.2
PFD[52]	95.5	89.7	83.0	81.5
KPR _{IN} [47]	95.9	89.6	85.4	79.1
KPR _{SOL} [47]	96.62	93.22	84.83	82.6
CLIP+ours	97.3	94.9	-	-
KPR _{IN} +ours	-	-	91	89.34

Table 9. Comparisons with state-of-the-art methods on Market1501 and Occluded-reID.

7.4. Collaborate with Re-ranking

Since our method does not change the features’ original distribution, it could collaborate post-processing strategies like rerank, as shown in Tab.7.

7.5. Results on MSMT17 with TransReID

We conduct a simple experiment on MSMT17 dataset with with TransReID and their official pre-trained weights. As shown in Tab.8.

7.6. Comparisons with state-of-the-art methods on three ReID benchmarks

Comparison on three ReID benchmarks. Since Our method can be applied to any baseline, we choose three methods from three benchmarks which have the official codes and pre-trained weights. With our method, we achieve the new SOTA in three benchmarks, as shown in Fig.9 and Fig.10.

7.7. Analysis on quality coefficient η of Generation Model

Fig.8 illustrates the effect of adjusting the coefficient η on the performance of the ReID model. To evaluate this impact, we gradually increased the value of η and observed changes on the mAP and Rank-1 metrics.

As the value of η increases, the performance of the ReID model improves, reaching an optimal point. At $\eta = 2$, both mAP and Rank-1 achieve their maximum values of 88.02% and 94.77%, respectively. However, further increasing η

Methods	All-Search		Indoor-Search	
	mAP	Rank-1	mAP	Rank-1
PMT[38]	66.13	67.70	77.81	72.95
MCLNet [15]	61.98	65.40	76.58	72.56
MAUM [37]	68.79	71.68	81.94	76.9
CAL[56]	71.73	74.66	83.68	79.69
SAAI(w/o AIM) [9]	71.81	75.29	84.6	81.59
SEFL[10]	72.33	77.12	82.95	82.07
PartMix[25]	74.62	77.78	84.38	81.52
MID [22]	59.40	60.27	70.12	64.86
FMCNet [67]	62.51	66.34	74.09	68.15
MPANet [57]	68.24	70.58	80.95	76.74
CMT [24]	68.57	71.88	79.91	76.90
protoHPE [64]	70.59	71.92	81.31	77.81
MUN [61]	73.81	76.24	82.06	79.42
MSCLNet [69]	71.64	76.99	81.17	78.49
DEEN [68]	71.80	74.70	83.30	80.30
CIFT [32]	74.79	74.08	85.61	81.82
SAAI+ours	76.44	79.33	86.83	84.2

Table 10. Comparison with state-of-the-art methods on SYSU-MM01 without re-ranking.

beyond this point leads to a slight decline in performance. It is easy to find that using generated images to centralize features is effective. However, considering the quality of the generated image, direct adding, although also effective, may not always achieve the best results. Therefore adjusting η according to the generation quality of the model in this dataset can better centralize the features.

7.8. Analysis on k_1/k_2 of Neighbor Feature Centralization

We conducted a detailed analysis of different k_1 and k_2 combinations, evaluating the results of feature centralization enhancement separately on the Query and Gallery sets, as well as the combined effect (as shown in the Fig.9). The selection of these two parameters primarily depends on the number of potential positive samples within the set (adjusting k_1) and the confidence in feature associations (adjusting k_2). Overall, medium parameter combinations (k_1 and k_2 in the range of 2-4) provide relatively optimal performance.